

Spray Deposition of Supercapacitor Electrodes using Environmentally Friendly Aqueous Activated Graphene and Activated Carbon Dispersions for Industrial Implementation

Nicolas Boulanger,^[a] Vasyl Skrypnychuk,^[a] Andreas Nordenström,^[a]
Gelínes Moreno-Fernández,^[b] Miguel Granados-Moreno,^[b] Daniel Carriazo,^[b, c]
Roman Mysyk,^[b] Gaetan Bracciale,^[d] Paolo Bondavalli,^{*,[d]} and Alexandr V. Talyzin^{*,[a]}

A spray gun machine was used to deposit high-surface-area supercapacitor electrodes using green non-toxic aqueous dispersions based on different kinds of high specific surface area nanostructured carbon materials: activated graphene (a-rGO) and activated carbon (AC). Tuning the spray conditions and dispersion formulation allowed us to achieve good adhesion to stainless-steel current collectors in combination with high surface area and a satisfactory mechanical stability of the electrodes. The specific surface area of approximately 2000 m²/g was measured directly on a-rGO and AC electrodes showing only around a 20% decrease compared to the precursor powder materials. The performance of the electrodes deposited on stainless-steel and aluminum current collectors

was tested in supercapacitor devices using three electrolytes. The electrodes were tested in an "as-deposited" state and after post-deposition annealing at 200 °C. The spray deposition method and post-deposition annealing are completely compatible with roll-to-roll industrial production methods. The a-rGO demonstrated superior performance compared to AC in supercapacitor electrodes with gravimetric capacitance, energy, and power density parameters, which exceed commercially available analogues. The formulation of the dispersions used in this study is environmentally friendly, as it is based on only on water as a solvent and commercially available non-toxic additives (graphene oxide, fumed silica, and carbon nanotubes).

1. Introduction

Energy storage is one of the key technological challenges of modern time. Electric double-layer capacitors (EDLC), also commonly named as supercapacitors, are devices, which store electricity by electrosorption using high specific surface area materials. Current industrial applications of supercapacitors

include for example engine starters (requiring high power in short time) and devices harvesting energy of slowing down vehicles (requires rapid charging). Nissan, Honda^[1] and Toyota^[2] have all experimented supercapacitors to complement the battery in hybrid vehicles.^[3] Supercapacitors were demonstrated to provide satisfactory performance to deliver power bursts in experimental fuel cell vehicles,^[4–5] and for emergency door opening in the Airbus 380 super jumbo jet.^[5] Supercapacitors store less energy compared to batteries (> 5 Wh/Kg), but deliver energy very quickly and therefore to show a very large specific power > 20 kW/Kg (for full packaged device). Moreover, they can be charged and discharged also more than 0.5–1 mln times due to the absence of chemical reactions involved.^[6–7]

In 1978, NEC went on to produce the first commercially successful double-layer capacitors.^[8] Currently, most of the commercial supercapacitors are produced using various kinds of nanostructured carbons, most commonly activated carbons which provide the best combination of textural and electrical properties. The first paper reporting carbon-nanotubes (CNT's) electrodes for supercapacitors was published in 1997 by Niu et al. of Hyperion Catalysis International and demonstrated that nanomaterials could improve capacitance and energy stored.^[9]


Graphene is a promising material for preparation of supercapacitor electrodes^[10] due to combination of high theoretical Specific Surface Area (SSA) (~2630 m²/g) and good conductivity.^[11] However, the high theoretical surface area is calculated for single layered graphene, while for practical applications it is necessary to prepare bulk materials. Graphene sheets demonstrate strong tendency to re-stack significantly


[a] Dr. N. Boulanger, Dr. V. Skrypnychuk, A. Nordenström, Dr. A. V. Talyzin
Department of Physics
Umeå University
Umeå, Sweden
E-mail: alexandr.talyzin@umu.se

[b] Dr. G. Moreno-Fernández, Dr. M. Granados-Moreno, Dr. D. Carriazo,
Dr. R. Mysyk
Centre for Cooperative Research on Alternative Energies (CIC energiGUNE)
Basque Research and Technology Alliance (BRTA)
Alava Technology Park
Albert Einstein 48, 01510 Vitoria-Gasteiz, Spain

[c] Dr. D. Carriazo
IKERBASQUE
Basque Foundation for Science
48013 Bilbao, Spain

[d] Dr. G. Bracciale, Dr. P. Bondavalli
Thales Research & Technology
1, avenue Augustin Fresnel
91767 Palaiseau, France
E-mail: paolo.bondavalli@thalesgroup.com

 Supporting information for this article is available on the WWW under
<https://doi.org/10.1002/celc.202100235>

 © 2021 The Authors. ChemElectroChem published by Wiley-VCH GmbH. This is an open access article under the terms of the Creative Commons Attribution License, which permits use, distribution and reproduction in any medium, provided the original work is properly cited.

reducing accessible surface. Most commonly used bulk material, powdered reduced graphene oxide (rGO), demonstrates much lower BET SSA values of 300–800 m²/g.^[12–13] The energy storage parameters of rGO based electrodes were reported with rather strong difference (e.g. 135–200 F/g)^[14–15] depending on specific synthesis methods or rGO preparation, electrode forming and details of measurements.

It is important to note that the SSA values are most often reported only for precursor materials rather than for ready-to-use electrodes. However, SSA typically decreases significantly in most of the procedures required for preparation of electrodes depending on rGO re-stacking.^[16–17]

Unlike rGO, the “activated graphene” (a-rGO) has a rigid 3D structure and well-defined pore size. The material is prepared using KOH activation of rGO obtained by explosive thermal or microwave exfoliation. The unique combination of high surface area (~3000 m²/g), easily accessible hierarchical porosity, high conductivity and mechanical stability make activated graphene a very attractive candidate for supercapacitor applications.^[18–21] Gravimetric electrode capacitance values in the range of 90–326 F/g have been reported for supercapacitors prepared using a-rGO^[18–20,22–24] However, relatively complex procedures (e.g. vacuum filtration of unstable suspensions)^[25] have been reported for preparation of a-rGO electrodes.

The dispersions based on organic solvents and other Graphene Related Materials (GRM) have been reported as a precursor for electrode preparation using e.g. spray deposition, ink jet printing or simple brush/blade deposition.^[26–30] The most common approach to prepare stable dispersions of hydrophobic graphene relies on liquid phase exfoliation in organic solvents, which are most often rather toxic and undesirable for industrial applications due to environmental concerns.^[31] Strongly hydrophobic nature of graphene^[32–33] and a-rGO^[34] was the main obstacle to preparation of stable water-based dispersions. Recently we developed new approach which allows to prepare stable water dispersions using filler hydrophobic materials (a-rGO and rGO) with micrometer size particles using graphene oxide as a main dispersion agent.^[35] Carbon nanotubes (CNT's) addition is used to improve mechanical properties of electrodes and to create electrical contact between a-rGO grains. Moreover, the electrical conductivity could be further improved by annealing the electrodes over the point of GO reduction thus providing additional electrical contact between particles of high surface area materials.^[35] These dispersions were demonstrated to provide excellent electrodes for supercapacitors after simple drying over the suitable current collector foil. The electrodes prepared using a-rGO filler demonstrated high surface area of ~1700 m²/g directly after deposition and high gravimetric/volumetric capacitance values. However, the electrodes were prepared using only small laboratory scale methods (brush/blade deposition) not suitable for industrial application. Here we demonstrate that liter amounts of a-rGO and activated carbons can easily be prepared and spray coated on current collectors to prepare supercapacitors.

Using aqueous dispersions paves the way to implement these new materials into industrial production as it allows reducing the fabrication costs and to make easier their

implementation for suitable industrial electrode preparation methods, such as spray deposition.

Spray-gun deposition method for supercapacitors was firstly demonstrated at UCLA in 2009 by Kaempegen et al. to fabricate CNT's based electrodes after putting nanomaterials in suspensions using specific solvent and spraying on PET substrates.^[36] The spray-gun used was static and the fabrication was lab-scaled. In 2013 Bondavalli et al. at Thales Research and Technology showed for the first time the deposition of nanomaterials using the dynamic spray-gun deposition method able on larger surfaces (15 cm × 15 cm).^[37] In this case substrate was heated at the boiling point of the solvent to avoid the so-called Coffee-ring effect on its surface. Thanks to immediate evaporation of solvent at the hot plate the nanomaterials are stuck at the point where they impact the substrate. It was demonstrated that this technique was suitable to fabricate electrodes for supercapacitors based on CNT's^[38] or mixtures of graphene/graphite and CNT's. The main advantage of spray gun deposition is that it can be easily implemented in roll-to-roll devices and so to allow the industrial fabrication of devices exploiting the great potential of new nanomaterials without raising the production costs. Some years after in 2017, two teams from IIT and Thales research and Technology were able to demonstrate a prototype of graphene based supercapacitor for mobile charger using spray deposition on commercial aluminum based collectors using activated carbon (AC)/graphene mixtures in iso-propanol (IPA). This was the first supercapacitor pre-industrialized prototype fabricated using this technique in the world.^[39–40] This was possible thanks to a new machine developed in the frame of the Graphene Flagship project, an EU initiative structuring the research on 2D nanomaterials, that has allowed achieving supercapacitors based electrodes based on graphene with dimensions of 30cmx30 cm. This is the state-of-the-art in term of dimension for fabrication of electrodes through this technique.

Here we will demonstrate for the first time the fabrication of graphene based electrodes using dynamic spray-gun deposition on a large surface and this for water based suspensions. Using graphene oxide as a surfactant allows to produce stable aqueous dispersions using almost any high surface area granular hydrophobic materials. In this study we demonstrate dispersions based on activated graphene and activated carbon. Activated graphene demonstrated superior gravimetric performance in supercapacitors, while activated carbons are beneficial due to mass production and low cost. This could be a major step for a greener fabrication process for electrodes avoiding the utilization of toxic solvent (e.g. Dimethylformamide, N-Methyl-Pyrrolidone^[41–42]) making easier the implementation of this technique in industrial plants and so for large scale and volume fabrication.

2. Results and Discussion

The goal of this study was to design simple industry-compatible method to deposit high SSA electrodes for supercapacitors using spray gun machine (Figure 1). The machine enables

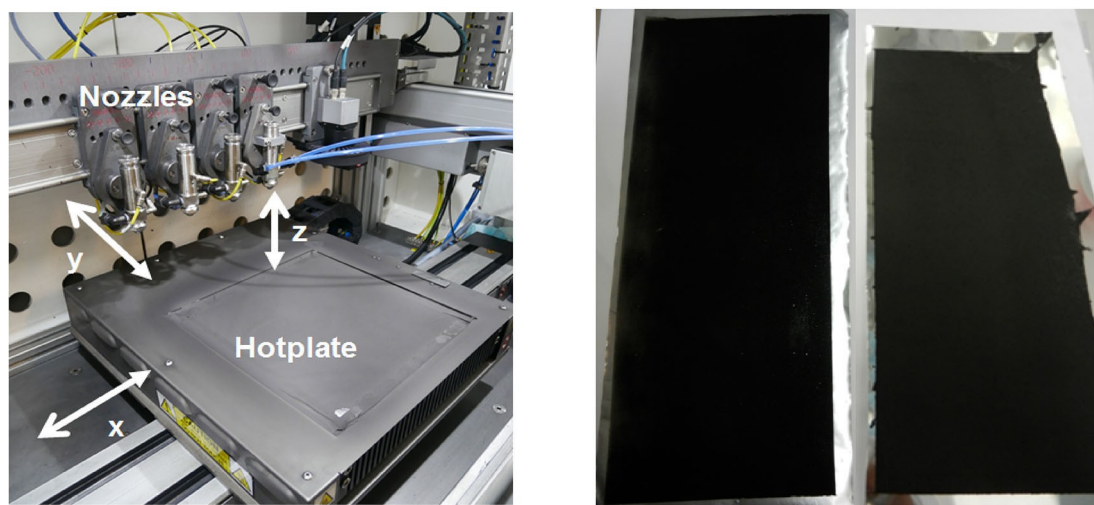


Figure 1. a) Spray-gun deposition set-up. b) Examples of carbon electrodes sprayed on metallic foils: aluminum (left) and Inox (right).

deposition of dispersions over large area current collector foils. The main challenge was to design water based formulations for specific conditions of spray deposition so that supercapacitor electrodes are formed directly after dispersion drying on current collectors. Three main parts of the process are described below: design of formulations for aqueous dispersions of high surface area carbon materials, optimization of spray gun deposition conditions and electrochemical characterization of supercapacitor electrodes.

2.1. Stable Aqueous Dispersions for Spray Deposition

The high surface area a-rGO and AC dispersions used for spray deposition were prepared using approach developed in our previous study.^[35] The high surface area carbon materials are hydrophobic, composed by micrometer size grains and cannot be directly dispersed in water. Fumed silica and graphene oxide were added to stabilize hydrophobic materials in water dispersion. CNT's were used to provide electrical contact between main material grains and to improve mechanical properties of electrodes. GO adsorbs well on CNT's surface because of co-existence of randomly distributed nm sized hydrophilic and hydrophobic areas within GO sheets.^[43–44] The ability of highly flexible GO to wrap/envelope both hydrophobic (a-rGO, CNT's) and hydrophilic particles (SiO_2) help to improve stability of dispersions.

Furthermore, electrically insulating GO can easily be converted into more conductive rGO using relatively mild heat treatment.^[45–46] Therefore, GO is not only helping to stabilize the dispersions but also useful component of electrode materials. Thermal reduction of GO at 200–250 °C results in formation of conductive rGO. The rGO sheets provide additional mechanical and electrical contact between the grains of high surface area carbons.^[35]

Simple drying of the dispersion on current collector foils allows to prepare electrodes which maintain high specific

surface area of the precursor material ($\sim 2000 \text{ m}^2/\text{g}$ measured on electrode). The electrodes are flexible thanks to the structure consisting of micrometer sized a-rGO or AC grains interconnected by carbon nanotubes. The dispersions are compatible with main industrial methods of electrode deposition such as brush/blade deposition, spray coating and ink jet printing. Moreover, the electrodes prepared using the coated dispersions provide gravimetric and volumetric capacitance values similar to powder-based a-rGO electrodes after simple laboratory scale blade deposition ($\sim 180 \text{ F/g}$).^[35] Here we scaled up preparation of dispersions to liters and tested spray gun deposition of supercapacitor electrodes.

The a-rGO and AC dispersions were prepared in 2 L amounts (2.5–5 mg/ml) to enable several spray deposition tests using the same batch. The dispersions are black in color and not transparent. Visual observations showed that all dispersions are stable during shelf storage with little precipitation on the bottom of bottles even after 2–3 days. The spray tests with 250 ml volume were performed to evaluate best deposition parameters.

2.2. Spray Deposition of Dispersions

Several parameters had to be optimized to prepare electrode materials by spray deposition, including nozzle speed, dispersion concentration and flow speed, temperature of substrate (aluminum or stainless-steel foils). The nozzles move on parallel lines (30 cm length) at 0.5 cm of distance to achieve the best uniform deposition. Indeed, the nanomaterials deposited have a Gaussian distribution centered on the nozzle position on the collector. The maximum speed of the nozzles 2 cm/s, nitrogen carrier gas pressure 3 bars and flow rate 25 ml/min were used. Concentration of the dispersions is one of the most fundamental parameters which require optimization. The final objective is to implement spray process for industrialized fabrication of supercapacitors. High concentration of nanomaterials in the

dispersions is desirable for rapid manufacturing of electrodes as it allows to achieve a sufficient loading in a reduced time. Previously tested dispersions deposited using a smaller two nozzles-machine were typically operated with concentrations at around 0.5 mg/ml. Here higher concentrations of water-based suspensions (20 g/l, 10 g/l, and 5 g/l) were tested. The first two failed due to clogging of the nozzles and for concentrations of 5 g/l we have been able to achieve some sample suitable for testing in supercapacitors. However, the sedimentation of the nanomaterials in the pipe moving from the reservoir through the pump to the nozzle was still an issue even with a 5 mg/ml concentration. This problem prevented reproducible multiple depositions due to periodical need for stopping the process and cleaning the nozzles and the pipes. For this reason, the concentration of dispersions was reduced to 2.5 g/l. In this case reproducible depositions were successfully performed without clogging. We note that the concentration of the dispersions is the parameter related to the size of nozzles, in our case orifice diameter of 1.3 mm. This is the optimized dimension considering quite high concentration of the nanomaterials and the high rate of the deposition process allowing a suitable and uniform deposition.

Rapid evaporation of solvent is required for preparation of homogeneous electrode films in the process of spray deposition. The evaporation rate is controlled using temperature of substrate. The first deposition tests with aqueous dispersions were performed using aluminum foil with temperature of ~130 °C. However, best results were achieved using higher temperature of 200 °C. The temperature above boiling point of water is needed due to the local decrease of temperature in process of deposition and incomplete solvent evaporation at lower temperatures. The optimal substrate temperature depends also on the quantity of liquid sprayed (quite important considering the nozzle orifice and the flow pressure) and by the latent heat. For this reason, the temperature was increased to 200 °C. Quite uniform depositions on both aluminum and stainless-steel foils at this temperature. The dispersions based on a-rGO and activated carbon sprayed on 200 °C hot plate were deposited using uniform deposition conditions and provided homogeneous electrodes. We have elaborated a process which allows us to fabricate several electrodes with the same deposition parameters with nearly the same mass. This process can be easily implemented in roll-to-roll without stopping the machine for maintenance.

Large area foils were cut on smaller pieces for testing for electrochemical performance in supercapacitors (Figure 2).

2.3. Characterization of Electrodes Prepared using Spray Deposition

The electrodes were characterized using XRD, Raman spectroscopy and TGA. As expected, XRD showed nearly amorphous nature of electrode materials with traces of graphitic carbon (Figure S1 in SI). Raman spectra recorded from the electrodes is simple combination of spectra from individual components exhibiting D and G bands from carbon materials (Figure S2 in

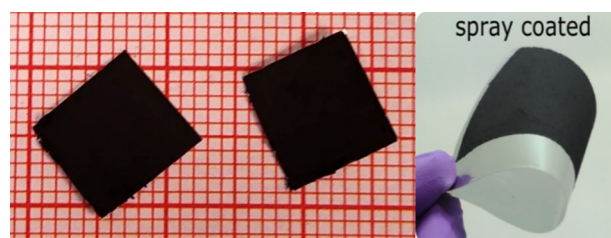


Figure 2. Electrodes sprayed on steel substrate and cut on pieces to test in supercapacitors.

SI). TGA tests performed under air allow to monitor reduction of GO with main step in weight loss at around 190 °C and to determine the amount of non-carbon components in the material (SiO₂) after oxidation of all carbons and evaporation from the sample in a form of CO₂ (see Figure S3 in SI file). TGA of annealed electrodes does not show a weight loss step typical for de-oxygenation of GO providing evidence that 200 °C temperature is sufficient for thermal deoxygenation of GO.

The complex composition of electrodes results in limited information obtained even after detailed analysis of characterization data, but we do not find any evidence for strong modification of individual components after all steps of dispersion preparation, deposition and drying. The electrode material can be considered as a simple sum of individual components.

As expected, SEM images of spray deposited electrodes showed that they consist of micrometer sized grains interconnected by CNT's and GO sheets. The electrode surface was homogeneous and reasonably smooth for the grainy materials like a-rGO and AC (Figure 3). Conductivity tests on annealed a-rGO based electrode piece removed from the current collector showed 530 S/m which is in good agreement with conductivity of a-rGO electrodes reported earlier for compressed powder material (500 S/m).^[20]

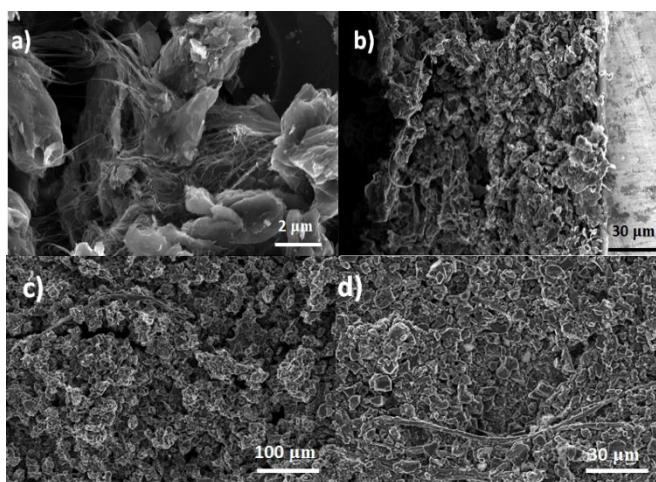


Figure 3. SEM images of a-rGO electrodes spray-deposited on current collector foil: a) micrometer size grains interconnected by CNT's; b) edge view of electrode attached to the substrate; c) top view of a-rGO electrode; d) top view of AC electrode.

The micrometer-scale particle size is essential property of aqueous dispersions used in this study for spray deposition. The 3D porous structure of the particles provides high surface area of electrodes. The pristine a-rGO and AC powders exhibit BET (cumulative) surface areas of 2583 m²/g (2148 m²/g), and 2581 m²/g (2062 m²/g) respectively (Figure S4 in SI). However, the surface area of final electrodes unavoidably decreases due to addition of components required for preparation of dispersions and all operations required for deposition. The balance between maximal surface area and satisfactory stability of the dispersions, good adhesion to current collector and mechanical stability has to be found to expect an implementation in real devices. The spray-coated electrodes were found to keep most of the original high surface area of precursor materials, 2034 m²/g for a-rGO and 1972 m²/g for AC. (Figure 4). The pore size distribution recorded from electrode materials is similar to the one for precursor, thus confirming that a-rGO and AC particles are essentially unchanged after preparation of dispersion and spray deposition. The surface area and pore size distribution of both a-rGO and AC electrodes remain also almost unchanged after post deposition annealing at 200 °C.

The surface area and pore size distribution are similar for electrodes annealed at 200 °C and not annealed (as deposited) electrodes. Remarkably, the BET surface areas of a-rGO and AC electrodes are almost the same but pore size distribution is different. AC electrodes demonstrate larger part of pore volume in micropores with size below 2 nm whereas a-rGO shows strong peak due to pores with ~3.4 nm width. The difference in a pore size distribution is likely to be responsible for difference in performance of electrodes tested in supercapacitor devices.

2.4. Performance of Electrodes Spray Coated using Aqueous Dispersions in Supercapacitors

The performance of a-rGO electrodes prepared by coating and drying aqueous dispersions (with and without post deposition annealing) was evaluated using a two-electrode supercapacitor setup in aqueous electrolyte (6 M KOH) and organic electrolyte (1 M TEA-BF₄ in acetonitrile). Relatively high values of specific current, and CV curve shapes close to rectangular were observed directly after coating using non-annealed a-rGO electrodes. Post deposition annealing of electrodes improved performance in all parameters of supercapacitors for all studied carbon materials.

Supercapacitors prepared using a-rGO electrodes demonstrated superior gravimetric performance compared to reference electrodes prepared using standard commercial activated carbon. Figure 5 shows data for annealed and non-annealed a-rGO and AC electrodes at a rate of 100 mV/s for the cyclic voltammetry (a,c) and charge-discharge data at a current density of 1 A/g (b,d). The deviation from a rectangular shape of the CV curve for both the activated carbon and activated reduced graphene oxide electrode (Figure 5) suggests some intrinsic resistance leading to a reduction in capacitance compared to the ideal case.

The CV curve for the annealed a-rGO electrode shows a shape almost ideally close to rectangular suggesting lower cell resistance. The measured specific capacitive current is also greater for the annealed electrode, implying increased charge storage. Annealing results in reduction of GO and improved electrical contact between the grains composing the electrodes.

This is reflected also in the CCCD curves shown Figure 5b, showing a longer discharge time (i.e., the higher capacitance)

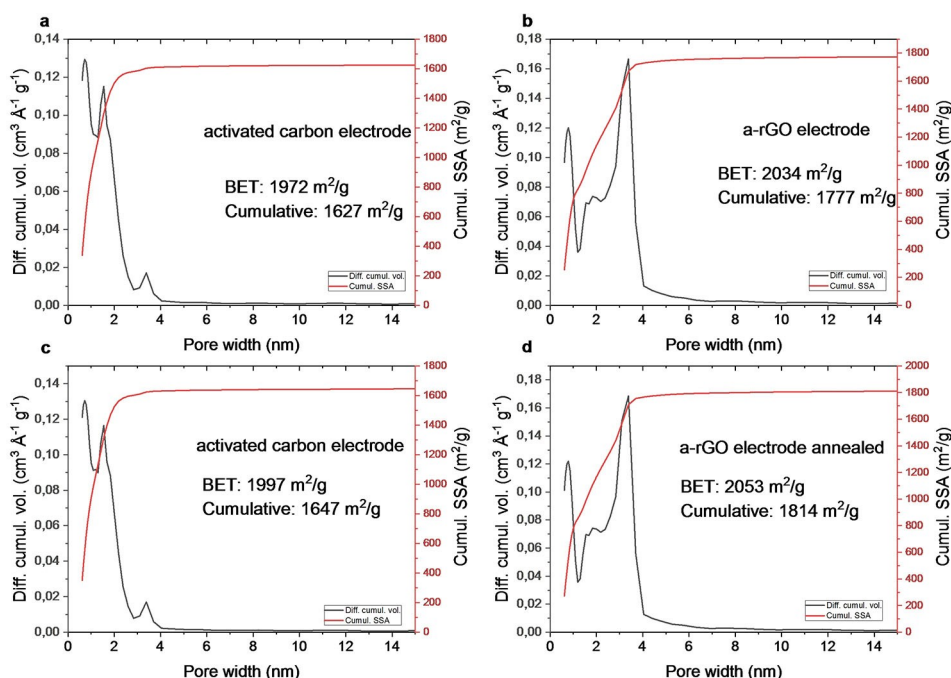


Figure 4. Cumulative pore volume and pore size distribution plots calculated using nitrogen sorption isotherms and QSDFT model for AC and a-rGO electrodes removed from current collectors. All electrodes are prepared using 10:1:1:1 (filler:GO:CNT:SiO₂) formulation.

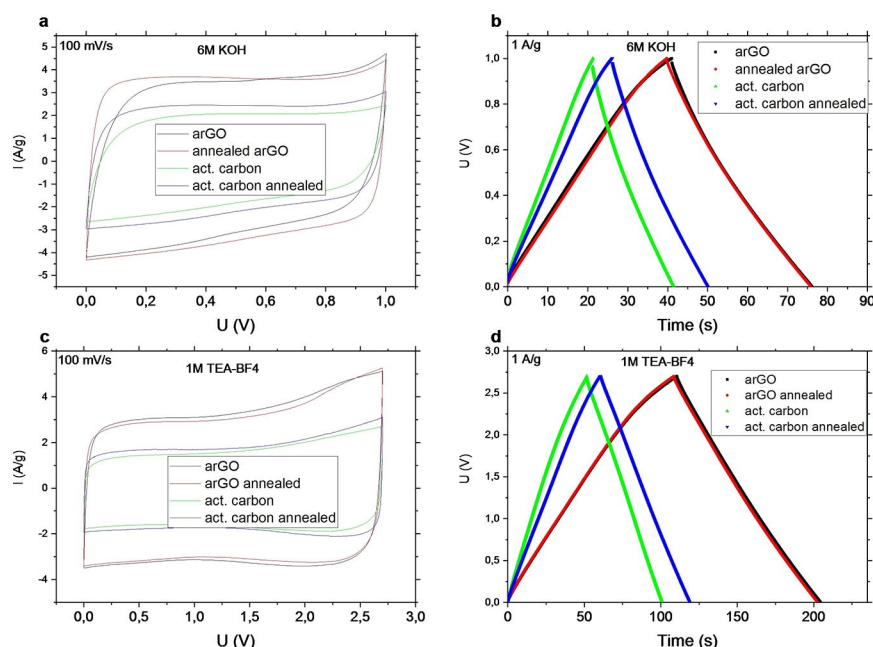


Figure 5. Cyclic voltammetry (a, c) and charge-discharge (b, d) curves for the activated carbon (green), annealed activated carbon (blue), activated reduced graphene oxide (black), and annealed activated reduced graphene oxide (red) electrodes. Each measurement was performed in 6 M KOH aqueous electrolyte (a, b) on a 0–1 V range as well as in 1 M TEA-BF₄ in acetonitrile organic electrolyte on a 0–2.7 V range.

for the annealed a-rGO electrode (36 seconds) compared to the activated carbon electrode (20 seconds, 44% faster), to the annealed activated carbon electrode (24 seconds, 33% faster), or to the non-annealed a-rGO electrode (35 seconds, 3% faster).

The CV curves show a much more rectangular shape, suggesting better conductivity when using a 1 M TEA-BF₄ in acetonitrile electrolyte (Figure 5c). Figure 5d shows the charge-discharge curves for the different electrodes. The discharge time for the electrodes when using 1 M TEA-BF₄ in acetonitrile as electrolyte is 94 seconds for the annealed a-rGO electrode, 94 seconds for the a-rGO electrode, 50 seconds for the activated carbon electrode, and 58 seconds for the annealed activated carbon electrode.

Figure 6a shows the Nyquist plots recorded for all a-rGO and AC electrodes in most industrially important organic electrolyte. The plots were measured for frequencies ranging from 100 kHz to 0.1 Hz with 10 frequencies measured per decade. The applied voltage was oscillating centered at 0 V with an amplitude of 10 mV. The first few points at high frequencies were discarded as the measured data was very noisy. Annealing of the electrodes resulted in a reduced impedance compared to non-annealed electrodes. Figure 6b and c show real and imaginary capacitance components calculated according to Ref. [47] where half $C''(F)$ and maximum $C''(F)$ correspond to the frequency reciprocal to characteristic capacitor response time τ , which is defined as the point of the 50% maximum energy loss and is related to the supercapacitor factor of merit. The values for organic electrolyte are quite low, between 1.58 s and 1 s for a-rGO materials, showing an improvement upon annealing, and 0.31 s for both activated carbons. The slightly higher values for a-rGO compared to those

for activated carbon are related to the higher capacitance of a-rGO since the other parameters are kept similar during electrode and cell preparation.

The values of τ are sufficiently low, thus allowing the validation of the developed electrode dispersions for the preparation of supercapacitor electrodes as confirmed by the blade-casting method.

The maximum capacitance obtained in 6 M KOH electrolyte, for a discharge current of 0.5 A/g is around 77 F/g for the activated carbon electrode, 88 F/g for the annealed activated carbon electrode, 129 F/g for the a-rGO and 134 F/g for the annealed a-rGO electrode. This capacitance value decreases with increasing discharge current, dropping to 49 F/g for the activated carbon electrode at 15 A/g (36% reduction), 51 F/g for the annealed activated carbon electrode at 30 A/g (42% reduction), 83 F/g for the a-rGO electrode at 40 A/g (36% reduction) and 107 F/g for the annealed a-rGO electrode at 40 A/g (20% reduction). The loss of capacitance is lower for the annealed a-rGO electrode compared to the non-annealed one, suggesting the annealing process not only improved the specific capacitance of the electrode but also its stability when used at high charge discharge currents. The effect of annealing is related to reduction of GO and smaller oxygen content in the sample.

The maximal capacitance measured in 1 M TEA-BF₄/acetonitrile electrolyte is 77 F/g at 0.5 A/g for the activated carbon electrode dropping to 45 F/g at 100 A/g (42% reduction), the annealed activated carbon electrode reached 86 F/g at 0.5 A/g and dropped to 59 F/g at 100 A/g (31% reduction), the a-rGO electrode showed a capacitance of 131 F/g at 0.5 A/g, reduced to 71 F/g at 100 A/g (46% reduction), and finally, the

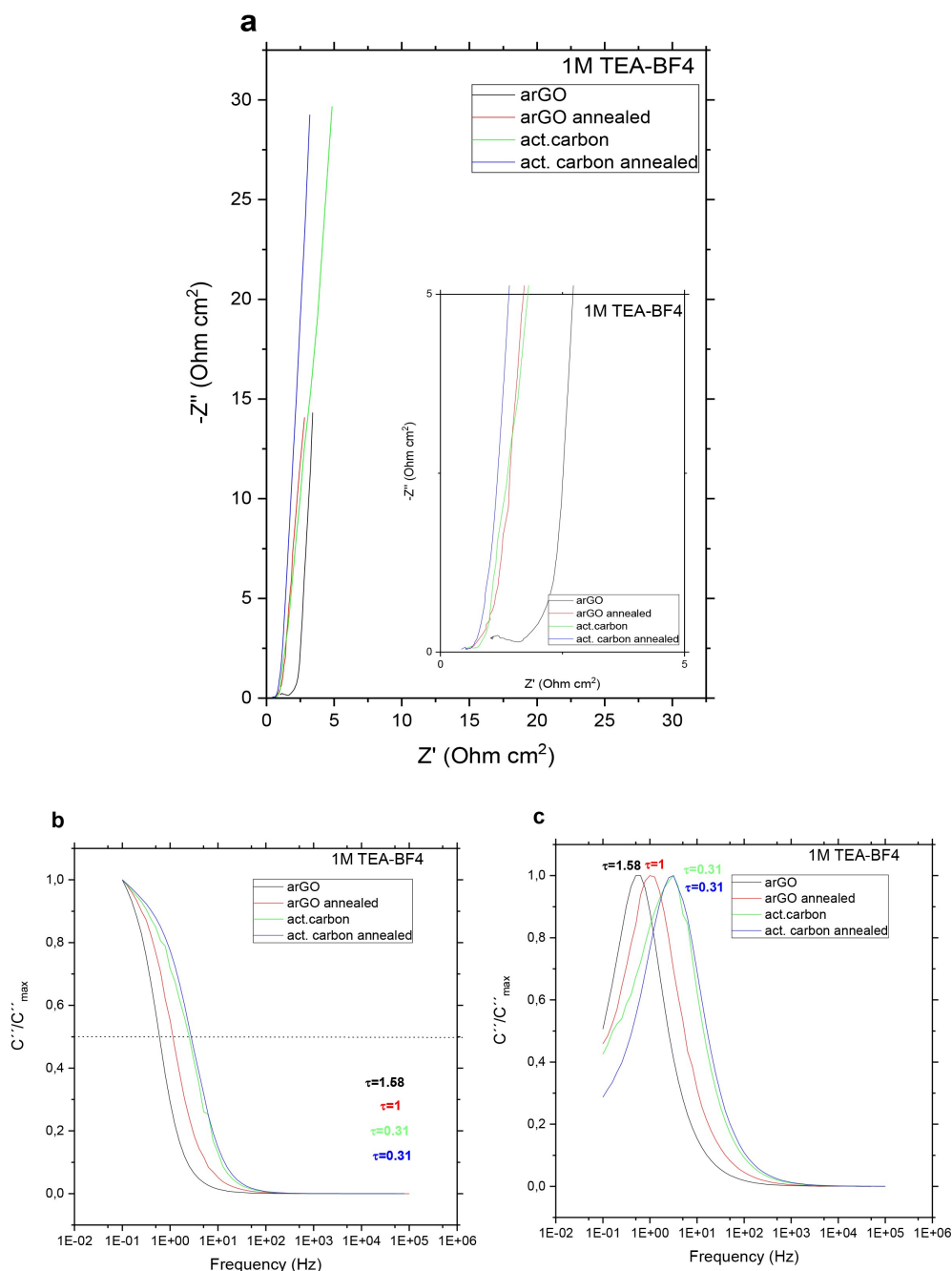


Figure 6. Nyquist plot for the different electrodes measured in 1 M TEA-BF₄ in acetonitrile organic electrolyte (a), real (C') (b), and imaginary (C'') vs. frequency graphs.

annealed a-rGO electrode started at a capacitance of 130 F/g at 0.5 A/g, down to 84 F/g at 100 A/g (35% reduction). Once again, annealing of the electrode improved its stability at higher discharge currents.

The performance in 6 M KOH aqueous electrolyte and 1 M TEA-BF₄ is compared in Figure 7 for AC and a-rGO electrodes with and without post-deposition annealing at 200 °C. The measurements were done based on constant current charge/discharge (CCCD) curves using current densities ranging from 0.5 A/g to 100 A/g. The capacitance values were obtained by integration of the discharge curve for each measurement.

As expected, tests performed in organic electrolyte show higher energy density compared to the measurements done in aqueous electrolytes. This is due to the use of a wider potential window for the charge/discharge of the electrodes, as measurements in aqueous electrolyte were done in a 0–1 V window while the organic electrolyte used a 0–2.7 V window. The energy density E is calculated as Equation (1):

$$E = \frac{1}{8} C_{el,sp} (U_{max}^2 - U_{min}^2) \quad (1)$$

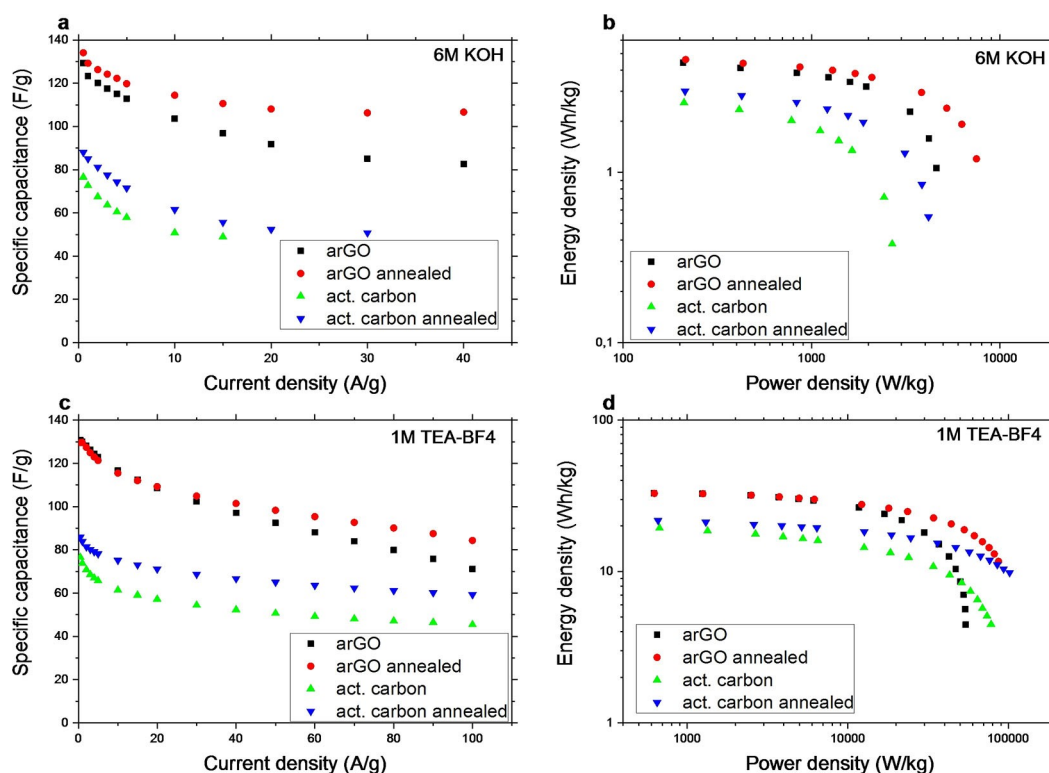


Figure 7. Specific capacitance as a function of current density (a, c) and Ragone plot (b, d) for the three different electrodes in 6 M KOH in water (a, b) and 1 M TEA-BF₄ in acetonitrile (c, d). The activated carbon based electrode is in green triangles, the annealed activated carbon based electrode is in blue inverted triangles, the activated reduced graphene oxide (a-rGO) based electrode is in black squares and the a-rGO based electrode after 1 hour annealing at 200 °C in air is in red circles.

where $C_{el,sp}$ is the specific capacitance of the electrode, U_{max} is the voltage at the beginning of the discharge, and U_{min} is the voltage at the end of the discharge (typically 0 V).

It is interesting also to compare electrodes prepared using spray and blade deposition. Figure 8 shows the Nyquist plot in high frequency range for the cells prepared using the non-annealed blade-deposited electrodes and the spray-deposited

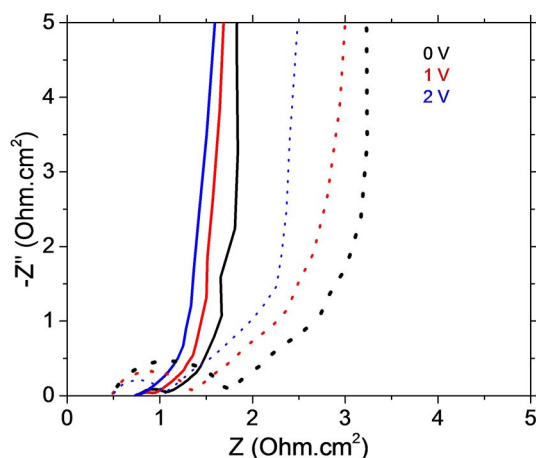


Figure 8. Nyquist plots in the high-frequency range for the non-annealed blade-deposited electrodes (dotted lines) and the spray-deposited electrodes (solid lines) measured in 1 M TEA-BF₄ in acetonitrile at different cell potential.

electrodes. In both cases, polarization to different cell potentials specifically highlights the transformation that the electrode composition undergoes depending on the material deposition method. When direct blade deposition is used, the Nyquist plots display a high-amplitude high-frequency semicircle. It is usually indicative of a poor electrode material/electrolyte interphase detrimental to rate response. Most often, such a semicircle originates from the presence of a passive coating, e.g. a native dielectric oxide layer on non-optimally selected current collectors, limiting ohmic coupling between the current collectors and the material. However, this is not the case since the semicircle changes substantially with potential (Figure 8), indicating charge transfer rather than an interphase resistance.^[48] This is not surprising since the electrode contains GO being able to exhibit charge transfer due to the presence of functional groups. However, the semicircle effect is substantially less noticeable for the cell made using the spray-deposited electrodes (Figure 8) where the semicircle has a much lower amplitude, and is virtually absent when the cell is polarized to 2 V. This is most likely due to the use of a hotplate during deposition at 200 °C, which partly reduces GO similarly to additional annealing at 200 °C for the bladed samples, thus minimizing their high-frequency resistance as described above. Therefore, using the temperature above the boiling point of the solvent in spray deposition allows not only abating the coffee-ring effect, but also improves the electrical properties of electrode composition with no need for a separate annealing

step, thus reducing the process flow. The sprayed electrodes not only result in the cells with a lower-amplitude semicircle, but also a less extended high-to-medium frequency sloping line, revealing the better electrode wetting with the electrolyte solution (Figure 8). This can be explained by the higher oxygen content of the more oxidized rGO being part of the non-annealed bladed composition and delayed electrode wetting.

The performance of a-rGO electrodes prepared using large area spray deposition was compared with electrodes prepared using standard laboratory scale blade deposition (Figure 9). Not very surprising, the small laboratory scale deposition provides electrodes with higher gravimetric capacitance (Figure 9a). However, performance of large scale spray deposited electrodes is not dramatically smaller, especially for TEA-BF₄ electrolyte (~22% smaller). Spray coated electrodes also demonstrated sharper downturn in energy density at high power density in the Ragone plot (Figure 9b). It needs to be noted that mass loading of bladed electrodes was about twice higher compared

to sprayed samples shown in Figure 9 and with equal thickness the difference between electrodes prepared using two methods would be somewhat stronger. The values obtained by blade deposition can be considered as a target for semi-industrial spray machine. Further tuning of spray deposition parameters is likely to decrease the difference and help to achieve the target values.

Characterization of a-rGO electrodes prepared by spray and blade deposition was also tested using both stainless-steel and aluminum current collectors with 1 M TEA BF₄/AN electrolyte.

Additional tests have been conducted to probe the suitability of the developed spray deposition method for current collectors made from different materials. Cyclic voltammetry graphs at different scan rates (Figure 10) show that spray deposition on Al leads to more resistive response as evidenced by the more extended capacitive current transient on switching polarization from negative to positive and *vice versa* (compare the CVs at 500 mV.s⁻¹). The Nyquist plots for the Al deposited sample shows a high-amplitude semicircle, pointing to the non-optimum interface or electrode composition. Since the semicircle amplitude does not significantly depend on cell potential, one can consider that the non-optimum response originates mainly from the passive coating on the surface of Al, most likely developed due to the temperature (200 °C) used in the spray deposition process. Despite a slightly higher resistance of the cells using Al current collectors, both Al and SS based electrodes lead to the same capacitance retention while deposition over Al leads to a slightly higher capacitance value (Figure 11a). This is also reflected in the Ragone plot (Figure 11b), demonstrating a somewhat higher energy density in the case of Al current collectors, but a more noticeable energy fade in the high-power region due to the worse Ohmic coupling with the Al current collectors. Thus, it can be concluded that spray deposition requires further tuning with respect to specific current collectors to preserve their interphase electrical properties. The procedure developed so far is rather optimized to stainless-steel current collectors. For comparison purposes, the Ragone plot of the cells using the best blade-deposited electrodes is also plotted to demonstrate the optimum performance that can be extracted using the same a-rGO based dispersions.

The basic properties and performance of electrodes prepared by spray deposition are summarized in the Table 1.

The data demonstrate that both kinds of tested high surface area carbon materials can be successfully implemented into aqueous dispersions which can be spray-deposited using semi-industrial machine on stainless-steel or aluminum large area current collector foils. The performance of supercapacitor electrodes improves significantly after annealing at 200 °C which converts electrically insulating GO into conductive rGO. The annealing step can easily be implemented in industry using e.g. roll to roll machine which pass the electrodes deposited on the foils through heated zone.

Remarkably, a-rGO electrodes demonstrated significantly higher gravimetric capacitance, volumetric capacitance and energy density compared to AC electrodes despite almost equal BET surface area of the precursor a-rGO and AC materials.

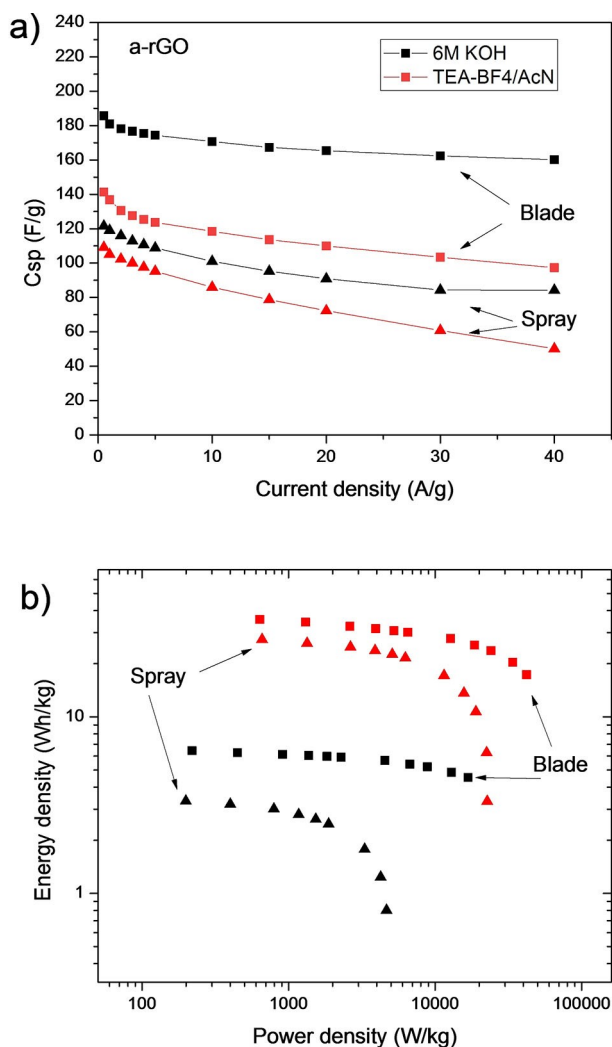


Figure 9. Gravimetric capacitance (a) and Ragone plot (b) for a-rGO electrodes deposited using the same dispersion by spray and blade deposition. Square symbols: blade deposition, triangles: spray deposition. Black symbols data recorded using 6 M KOH electrolyte, red symbols: data recorded using TEA-BF₄/ACN electrolytes. No post-deposition annealing applied.

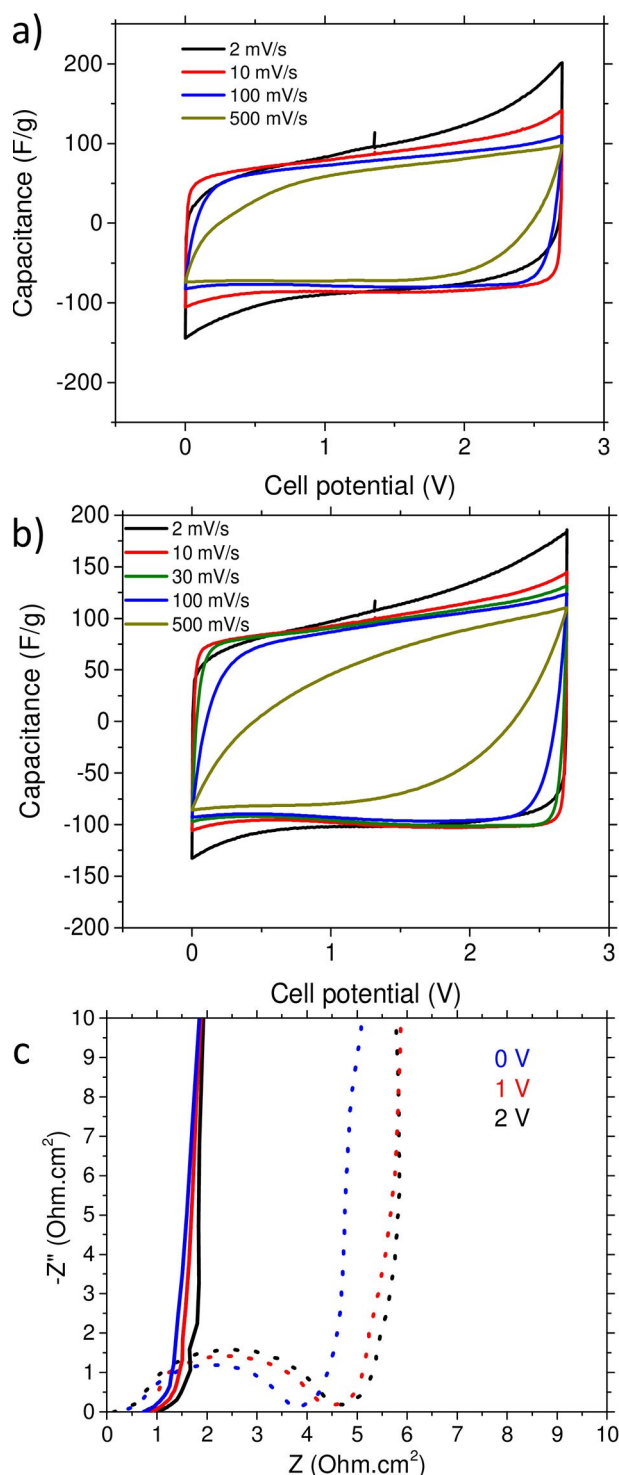


Figure 10. Comparative electrochemical characterization between the cells using spray deposited electrodes. Cyclic voltammetry for SS (a) and aluminum (b) current collectors, and high-frequency Nyquist plots (c) for stainless-steel (solid lines) and aluminum (dotted lines) current collectors at different cell potentials.

Therefore, results presented here provide immediate interest to spray deposition of supercapacitor electrodes based on AC available in industry scale and provides promising future outlook for using a-rGO which provides superior performance

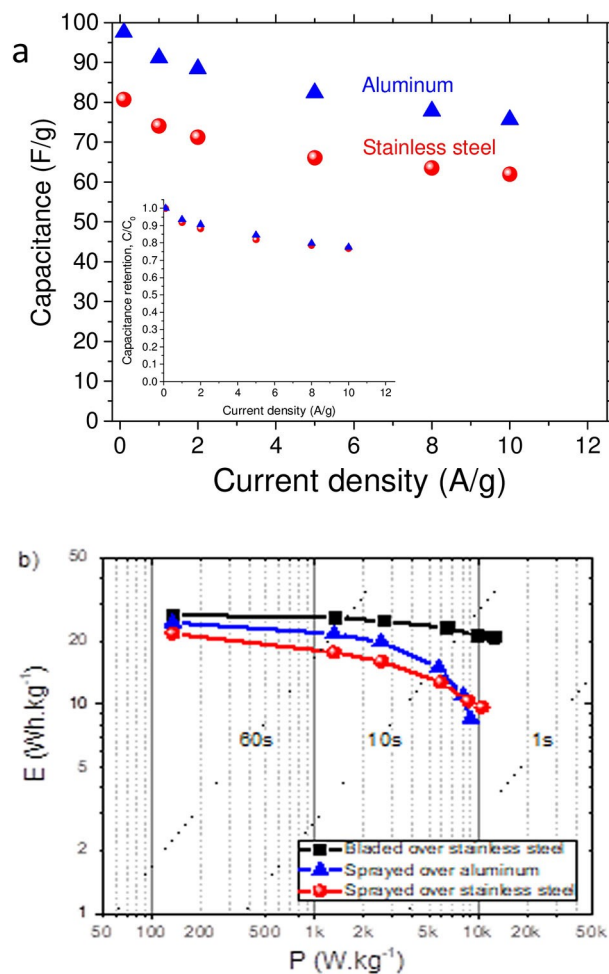


Figure 11. Comparison between bladed and spray-deposited a-rGO on stainless-steel and aluminum current collectors. Gravimetric vs current density of symmetric supercapacitor cells (the inset shows capacitance retention) of electrodes of (a) and Ragone plot (b).

but not yet available in industrial amounts. Most important, the whole process of electrode deposition is entirely green and environmentally friendly due to using aqueous dispersions. Using water for the dispersions allows to avoid expensive encapsulation and recycling technologies otherwise required to prevent contamination of environment with toxic solvents.

3. Conclusions

In conclusion, aqueous dispersions prepared using two kinds of high surface area nanostructured carbon materials (activated graphene and activated carbon) were spray gun deposited on stainless-steel and aluminum current collectors. The performance of electrodes was tested in supercapacitor devices using two electrolytes: aqueous and organic. The electrodes were tested in “as deposited” state and after post deposition annealing at 200 °C. The spray deposition method and post deposition annealing are completely compatible with roll to roll industrial production methods. Activated graphene demon-

Table 1. Summary for data related to electrochemical performance of spray-deposited electrodes in supercapacitors (with and without post deposition annealing) and surface area of precursors.

Filler material	AC	Annealed AC	a-rGO	Annealed a-rGO
SSA				
BET [m ² /g]	2581		2583	
Cumulative [m ² /g]	2062		2148	
Performance in 6 M KOH at 1 A/g				
Gravimetric capacitance [F/g]	73	85	123	129
Volumetric capacitance [F/cm ³]	30	31	51	50
Power density [W/kg]	413	426	420	433
Energy Density, [Wh/kg]	2.34	2.83	4.11	4.37
Performance in 1 A/g in 1 M TEA-BF ₄				
Gravimetric capacitance [F/g]	74	84	130	130
Volumetric capacitance [F/cm ³]	31	31	49	51
Power density [W/kg]	1343	1308	1247	1254
Energy density [Wh/kg]	18.5	21.2	32.6	32.6

strated superior to activated carbon performance in supercapacitor electrodes with high gravimetric/volumetric capacitance, energy and power density parameters which exceed commercially available analogues. The formulation of dispersions used in this study is environmentally friendly as it is based only on water as solvent and commercially available non-toxic additives (fumed silica and CNT's) which is an extremely important advantage for industrial implementation. While the activated graphene can be considered as a material of future currently available in limited few gram amounts, using industrial activated carbon in the proposed dispersion formulation allows production of electrodes using cost efficient spray deposition method in completely environmentally free process. Using water instead of organic solvents allows to avoid expensive steps for solvent recycling and confinement to avoid pollution of environment. Spray gun technique and dispersion formulations can be further tuned to achieve the maximal performance parameters of activated graphene evaluate using small laboratory scale methods of electrode repARATION.

Experimental Section

Materials

Two kinds of granular high surface area materials were studied here for preparation of aqueous dispersions and tested for spray gun deposition.

- 1) Activated graphene powder was prepared using KOH activation of rGO prepared by explosive exfoliation, details of preparation and characterization of this material are available

elsewhere.^[34–35] The synthesis was repeated several times and material was mixed together to produce one large batch of a-rGO which was later used for preparation of dispersions. The BET SSA of this batch was evaluated using analysis for nitrogen sorption as ~2600 m²/g (2150 m²/g using QSDFT model). The a-rGO material showed no diffraction peaks in XRD and low oxygen content (C/O=55 determined by comparing areas of C1s and O1s) according to XPS.^[35]

- 2) Activated carbon YP-80F by Kuraray Co., Ltd.

Nanocrystalline fumed silica was purchased from Sigma-Aldrich. We are grateful to OCSiAl for providing a sample of single walled carbon nanotubes (SWCNT) used in this study, BET SSA of these CNT's was measured to be 1180 m²/g. Graphene oxide was purchased from Abalonyx (Norway).

The aqueous dispersions were prepared first in few ml volume and applied to stainless-steel foils using blade deposition. Once reasonably good adhesion to the foil was observed, larger batches with volume up to 2 liters were prepared for spray deposition. The dispersions were prepared using four components: high surface area filler, graphene oxide, fumed silica, CNT's.

For activated carbon (AC) bulk samples of dispersion used later in spray deposition experiments was prepared using proportion of components 10:1:1:1 AC:GO:CNT: fumed silica nanoparticles mixture (by weight), a-rGO dispersion in a 10:2:1:1. The dispersions were prepared in concentration 2.5–5 mg/ml considering only filler amount.

The dispersions are prepared in three simple steps: 1) CNT's are dispersed in water using graphene oxide additive using 5 min ball milling. 2) Fumed silica is added in order to stabilize the dispersion and to tune its rheological properties. 3) high surface area filler material in powder form is added to the fluid mixture and milled for 5 min again. See details of the procedure elsewhere.^[35] Electrodes have been deposited by spray or blade deposition. Post deposition treatment using annealing in air for 1 hour at 200 °C has been done for some samples in order to reduce GO and to improve the electrode properties.

The a-rGO based electrode deposited using aqueous dispersion was accurately removed and studied using analysis of nitrogen sorption isotherms, Figure 4.

Spray Deposition

The dispersions were gun-sprayed on aluminum (Maxwell) and Inox collectors (Goodfellow) with thickness of 20 µm and 50 µm, respectively. The spray gun machine is shown in Figure 1. The moving spray-nozzle has a constant distance of ~15 cm from the surface. The collectors are placed on the hotplate and so stuck on it using vacuum. Then they are heated up to a temperature above the boiling point of water (> 100 °C) to ensure the instantaneous evaporation of the solvent droplets, thus avoiding the "coffee-ring" effect.^[49–50] This chuck can be moved together with the spray-gun in the X–Y plane. The nozzle height over the substrate can be finely adjusted. The precision for all the movements is around 100 µm. Thanks to the automatic deposition process, sequences have been computed with deposition taking place on lines with length of 30 cm and with a pitch of around 1 cm to allow the best recovery of the sprayed cones^[39] on a total width of 10 cm. The nozzles speed is of 2 cm/s and the nozzle overture of 1.3 mm. The carrier gas for nebulization of the suspension is nitrogen. We have elaborated a process which allows us to fabricate several electrodes with the same deposition parameters with nearly the same mass. These last can change as a function of the sprayed dispersion

composition. In order to verify the exact amount of material deposited, current collectors are carefully weighted (Perkin-Elmer AD-4 auto balance with an accuracy of ~ 0.02 mg) before and after spraying the graphene based dispersion. The dispersions stored for several days before deposition were mildly sonicated in a bath for 15 hours to improve stability and uniformity of the concentration between the top and the bottom of the bottle.

Electrode Characterization

X-ray diffraction (XRD) measurements were carried out on the assembled electrodes (substrate together with active material) as well as on the isolated substrates using Cu-K α radiation (X' Pert³ Powder, PANalytical) on a 2-Theta range of 3.5° to 55°, using a 1/16° fixed diffraction slit and a 2° fixed anti-scattering slit.

Thermogravimetric analysis (TGA) was carried out using a Mettler Toledo TGA/DSC1 STAR^e system. The sample mass was determined in the instrument at a set temperature of 25 °C (sample temperature of about 28 °C). The measurement was then started with first a stabilization step at a set temperature of 25 °C for 20 minutes followed by a ramp up to a set temperature of 800 °C at a speed of 1 °C/min.

Raman spectra were recorded on an Invia Raman spectroscopy (Renishaw) using a 514 nm laser with a 300 second acquisition time.

The specific surface area was evaluated by analysis of nitrogen sorption isotherms acquired using Autosorb iQ XR analyzer by Quantachrome. A slit pore quenched solid density functional theory (QSDFT) equilibrium model was used to evaluate cumulative SSA, pore volume and pore size distribution of the samples. SEM images were recorded using a Zeiss Merlin FEG-SEM microscope.

Testing Electrodes in Supercapacitors

Spray deposition over large area metal foils was used in this study. Typical electrodes are shown Figures 1, 2 showing good uniformity of the sprayed active material. In order to determine the mass of active material per electrode, a sacrificial electrode was cut and weighed. The active material was then removed, and the substrate was weighed again using a magnetic suspension balance (Rubotherm) (0.01 mg precision), allowing the determination of the weight ratio between the active material and the mass of the full electrode. The performance of a-rGO electrodes prepared by coating and drying aqueous dispersions (with and without post deposition annealing) was evaluated using a two-electrode supercapacitor setup in aqueous electrolyte (6 M KOH) and organic electrolyte (1 M TEA BF₄ in acetonitrile).

Typical electrode sizes are 1.3–1.5 cm² for electrodes measured in aqueous electrolyte and 0.5–1.0 cm² for electrodes measured in organic electrolyte, electrode mass loading is 1.4–1.8 mg/cm² (spray deposition) and 4–5 mg/cm² for blade deposition. For the data shown below in figures following mass loading was measured: blade coated a-rGO sample: ~ 5.2 mg/cm², Sprayed coated samples: activated carbon: 1.78 mg/cm², annealed activated carbon: 1.43 mg/cm², a-rGO: 1.90 mg/cm², annealed a-rGO: 1.85 mg/cm². The measurement stack was then prepared in the measurement cell, using a glass fiber separator (Whatman glass microfiber filter). In the case of the organic electrolyte, the stack was first stored overnight in an argon filled glovebox before introducing the electrolyte, in order to reduce the water content. Electrolyte was then introduced in the cell, in such amount as to saturate the glass fiber separator and the cell was then sealed. The capacitance measurement was performed using a potentiostat (Iviumstat XR,

Ivium) and Biologic VMP3. First, current-voltage (CV) curves were recorded in a range of 0 to 1 V (aqueous electrolyte) or 0 to 2.7 V (organic electrolyte). The sweep rates were 50 mV/s, 100 mV/s, 200 mV/s and 500 mV/s. Electrochemical impedance spectroscopy was carried out on a frequency range of 0.1–100000 Hz with an amplitude of 0.01 V centered at 0 V. Finally, charge-discharge (CD) curves were recorded from 0 to 1 V (aqueous electrolyte) or 0 to 2.7 V (organic electrolyte) at current densities ranging from 0.5 A/g up to 100 A/g. Details of calculations and analysis of measured data are provided in our earlier publications.^[34–35]

Acknowledgements

Authors acknowledge funding from the European Union's Horizon 2020 research and innovation program under grant agreement No785219 and No 881603. A.T. acknowledges support from Swedish Research Council grant (no. 2017-04173), acknowledge the Vibrational Spectroscopy Platform of Umeå University and A. Shchukarev for support with XPS test.

Conflict of Interest

The authors declare no conflict of interest.

Keywords: graphene · supercapacitors · spray deposition · electrodes · surface area

- [1] R. C. Bansal, *Handbook Of Automotive Power Electronics and Motor Drives*, edited by Emadi, A. (CRC press, Boca Raton, FL., 2005) 2005.
- [2] K. Miyadera, *Toyota Tech. Rev.* **2002**, 52 22–27.
- [3] P. Podatz, O. Garcia, L. Guzzella, F. Buchi, G. Scherer, A. Wokaun, *Conference proceedings SAE Int. Publ.* **2003**, 2003-2001–0418.
- [4] J. M. Tarascon, M. Armand, *Nature* **2001**, 414, 359–367.
- [5] P. Simon, Y. Gogotsi, *Nat. Mater.* **2008**, 7, 845–854.
- [6] V. V. N. Obreja, *Proceedings of the International conference on renewable energies and power quality* **2007**, 1, 531–535.
- [7] J. Miller, A. Burke, *The Electrochem. Soc.* **2008**, 17, 53–57.
- [8] J. M. Miller, *IEEE Vehicle Power* **2009**, 4–10.
- [9] C. M. Niu, E. K. Sichel, R. Hoch, D. Moy, H. Tennent, *Appl. Phys. Lett.* **1997**, 70, 1480–1482.
- [10] Y. L. Shao, M. F. El-Kady, L. J. Wang, Q. H. Zhang, Y. G. Li, H. Z. Wang, M. F. Mousavi, R. B. Kaner, *Chem. Soc. Rev.* **2015**, 44, 3639–3665.
- [11] F. Bonaccorso, L. Colombo, G. H. Yu, M. Stoller, V. Tozzini, A. C. Ferrari, R. S. Ruoff, V. Pellegrini, *Science* **2015**, 347.
- [12] R. Raccichini, A. Varzi, S. Passerini, B. Scrosati, *Nat. Mater.* **2015**, 14, 271–279.
- [13] Y. Q. Sun, Q. O. Wu, G. Q. Shi, *Energy Environ. Sci.* **2011**, 4, 1113–1132.
- [14] Y. W. Zhu, S. Murali, M. D. Stoller, A. Velamakanni, R. D. Piner, R. S. Ruoff, *Carbon* **2010**, 48, 2118–2122.
- [15] M. D. Stoller, S. J. Park, Y. W. Zhu, J. H. An, R. S. Ruoff, *Nano Lett.* **2008**, 8, 3498–3502.
- [16] Y. Wang, Y. P. Wu, Y. Huang, F. Zhang, X. Yang, Y. F. Ma, Y. S. Chen, *J. Phys. Chem. C* **2011**, 115, 23192–23197.
- [17] J. T. Li, M. Ostling, *Crystals* **2013**, 3, 163–190.
- [18] T. Kim, G. Jung, S. Yoo, K. S. Suh, R. S. Ruoff, *ACS Nano* **2013**, 7, 6899–6905.
- [19] S. Murali, J. R. Potts, S. Stoller, J. Park, M. D. Stoner, L. L. Zhang, Y. W. Zhu, R. S. Ruoff, *Carbon* **2012**, 50, 3482–3485.
- [20] Y. W. Zhu, S. Murali, M. D. Stoller, K. J. Ganesh, W. W. Cai, P. J. Ferreira, A. Pirkle, R. M. Wallace, K. A. Cychoz, M. Thommes, D. Su, E. A. Stach, R. S. Ruoff, *Science* **2011**, 332, 1537–1541.
- [21] A. Klechikov, G. Mercier, T. Sharifi, I. A. Baburin, G. Seifert, A. V. Talyzin, *Chem. Commun.* **2015**, 51, 15280–15283.

- [22] S. Murali, N. Quarles, L. L. Zhang, J. R. Potts, Z. Q. Tan, Y. L. Lu, Y. W. Zhu, R. S. Ruoff, *Nano Energy* **2013**, *2*, 764–768.
- [23] C. Zheng, X. F. Zhou, H. L. Cao, G. H. Wang, Z. P. Liu, *J. Mater. Chem. A* **2015**, *3*, 9543–9549.
- [24] Z. S. Wu, S. Yang, L. L. Zhang, J. B. Wagner, X. L. Feng, K. Mullen, *Energy Storage Mater.* **2015**, *1*, 119–126.
- [25] L. L. Zhang, X. Zhao, M. D. Stoller, Y. W. Zhu, H. X. Ji, S. Murali, Y. P. Wu, S. Perales, B. Clevenger, R. S. Ruoff, *Nano Lett.* **2012**, *12*, 1806–1812.
- [26] H. Q. Zheng, C. Y. Neo, X. G. Mei, J. Qiu, J. Y. Ouyang, *J. Mater. Chem.* **2012**, *22*, 14465–14474.
- [27] J. T. Li, F. Ye, S. Vaziri, M. Muhammed, M. C. Lemme, M. Ostling, *Adv. Mater.* **2013**, *25*, 3985–3992.
- [28] T. Carey, C. Jones, F. Le Moal, D. Deganello, F. Torrisi, *ACS Appl. Mater. Interfaces* **2018**, *10*, 19948–19956.
- [29] N. W. Pu, C. A. Wang, Y. M. Liu, Y. Sung, D. S. Wang, M. D. Ger, *J. Taiwan Inst. Chem. E* **2012**, *43*, 140–146.
- [30] B. Wang, J. Z. Liu, Y. Zhao, Y. Li, W. Xian, M. Amjadipour, J. MacLeod, N. Motta, *ACS Appl. Mater. Interfaces* **2016**, *8*, 22316–22323.
- [31] Y. Y. Xu, H. Z. Cao, Y. Q. Xue, B. Li, W. H. Cai, *Nanomaterials* **2018**, *8*.
- [32] J. Feng, Z. G. Guo, *Nanoscale Horiz.* **2019**, *4*, 339–364.
- [33] F. Taherian, V. Marcon, N. F. A. van der Vegt, F. Leroy, *Langmuir* **2013**, *29*, 1457–1465.
- [34] A. Iakunkov, V. Skrypnichuk, A. Nordenstrom, E. A. Shilayeva, M. Korobov, M. Prodana, M. Enachescu, S. H. Larsson, A. V. Talyzin, *Phys. Chem. Chem. Phys.* **2019**, *21*, 17901–17912.
- [35] V. Skrypnichuk, N. Boulanger, A. Nordenstrom, A. Talyzin, *J. Phys. Chem. Lett.* **2020**, *11*, 3032–3038.
- [36] M. Kaempgen, C. K. Chan, J. Ma, Y. Cui, G. Gruner, *Nano Lett.* **2009**, *9*, 1872–1876.
- [37] P. Bondavalli, C. Delfaure, P. Legagneux, D. Pribat, *J. Electrochem. Soc.* **2013**, *160*, A601–A606.
- [38] S. Tuukkanen, M. Valimäki, S. Lehtimäki, T. Vuorinen, D. Lupo, *Sci. Rep.* **2016**, *6*.
- [39] A. Ansaldo, P. Bondavalli, S. Bellani, A. E. D. Castillo, M. Prato, V. Pellegrini, G. Pognon, F. Bonaccorso, *ChemNanoMat* **2017**, *3*, 436–446.
- [40] Y. Hernandez, V. Nicolosi, M. Lotya, F. M. Blighe, Z. Y. Sun, S. De, I. T. McGovern, B. Holland, M. Byrne, Y. K. Gun'ko, J. J. Boland, P. Niraj, G. Duesberg, S. Krishnamurthy, R. Goodhue, J. Hutchison, V. Scardaci, A. C. Ferrari, J. N. Coleman, *Nat. Nanotechnol.* **2008**, *3*, 563–568.
- [41] P. Bondavalli, M. B. Martin, L. Hamidouche, A. Montanaro, A. F. Trompeta, C. A. Charitidis, *Micromachines-Basel* **2019**, *10*.
- [42] C. Pramanik, J. R. Gissinger, S. Kumar, H. Heinz, *ACS Nano* **2017**, *11*, 12805–12816.
- [43] C. Zhang, L. L. Ren, X. Y. Wang, T. X. Liu, *J. Phys. Chem. C* **2010**, *114*, 11435–11440.
- [44] L. Qiu, X. W. Yang, X. L. Gou, W. R. Yang, Z. F. Ma, G. G. Wallace, D. Li, *Chem. Eur. J.* **2010**, *16*, 10653–10658.
- [45] U. Hofmann, A. Frenzel, E. Csálán, *Justus Liebigs Ann. Chem.* **1934**, *510*, 1–41.
- [46] Z. Q. Wei, D. B. Wang, S. Kim, S. Y. Kim, Y. K. Hu, M. K. Yakes, A. R. Laracuente, Z. T. Dai, S. R. Marder, C. Berger, W. P. King, W. A. de Heer, P. E. Sheehan, E. Riedo, *Science* **2010**, *328*, 1373–1376.
- [47] P. L. Taberna, P. Simon, J. F. Fauvarque, *J. Electrochem. Soc.* **2003**, *150*, A292–A300.
- [48] T. S. Mathis, N. Kurra, X. H. Wang, D. Pinto, P. Simon, Y. Gogotsi, *Adv. Energy Mater.* **2019**, *9*.
- [49] R. D. Deegan, O. Bakajin, T. F. Dupont, G. Huber, S. R. Nagel, T. A. Witten, *Nature* **1997**, *389*, 827–829.
- [50] R. D. Deegan, O. Bakajin, T. F. Dupont, G. Huber, S. R. Nagel, T. A. Witten, *Phys. Rev. E* **2000**, *62*, 756–765.

Manuscript received: February 22, 2021
Accepted manuscript online: March 5, 2021